Single-Cell Mechanical Properties: Label-Free Biomarkers for Cell Status Evaluation

Jian Chen, Song-Bin Huang, Chengcheng Xue, Beiyuan Fan, Deyong Chen, Junbo Wang and Min-Hsien Wu

Abstract The mechanical behavior of biological cells is largely determined by their cytoskeletons; abnormal cellular functions can change cytoskeletons, leading to variations in cellular mechanical properties. This chapter begins with a summary of the relationships between cellular mechanical properties and various disease processes and changes in cell states: (1) changes in stiffness of red blood cells in cytoskeletal disorders, such as malaria and sickle cell anemia; (2) increased cell deformability of invasive cancer cells, compared with benign counterparts; (3) increased stiffness of leukocytes in sepsis; and (4) decreased deformability during the stem cell differentiation process. In the following section, we discuss the well-established techniques that are being used to measure the mechanical properties of single cells, including atomic force microscopy and micropipette aspiration. Finally, we describe the microfluidic approaches—including microfluidic constriction channels, microfluidic optical stretchers, and microfluidic hydrodynamic stretchers—that are being developed as next-generation, automated, and high-throughput techniques for characterization of the mechanical properties of single cells. The advantages and limitations of each technique are compared and future research opportunities are highlighted.

Keywords Single-cell analysis · Cellular mechanics · Characterization of single-cell mechanical properties · Microfluidics

J. Chen · C. Xue · B. Fan · D. Chen · J. Wang (✉)
State Key Laboratory of Transducer Technology, Institute of Electronics, Chinese Academy of Sciences, No.19 North 4th Ring Road West, Haidian District, Beijing, People's Republic of China
e-mail: jbwang@mail.ie.ac.cn

S.-B. Huang · M.-H. Wu (✉)
Graduate Institute of Biochemical and Biomedical Engineering, Chang Gung University, No. 259, Wenhua 1st Road, Guishan District, Taoyuan City, Taiwan
e-mail: mhwu@mail.cgu.edu.tw

F.-G. Tseng and T.S. Santra (eds.), *Essentials of Single-Cell Analysis*, Series in BioEngineering, DOI 10.1007/978-3-662-49118-8_8

1 Introduction

The mechanical behavior and properties of a eukaryotic cell are largely determined by the characteristics of its cytoskeleton, an elaborate network of fibrous proteins [1, 2]. More specifically, the deformability of nucleated cells is determined by the membrane, the cytoskeletal network (actin filaments, intermediate filaments, and microtubules), and its interaction with the nucleus. Incompressible viscoelastic solids with key parameters of $E_{instantaneous}$ and $E_{equilibrium}$ are proposed to model these nucleated cells. As to the deformability of red blood cells (RBCs), it is determined by the membrane skeleton network, which is modeled as cortical shell-liquid core (or liquid drop) models [3]. Abnormal cellular functions can change cytoskeletons and lead to variations in mechanical properties of cells [4, 5].

This chapter summarizes the relationships between cellular mechanical properties and various disease processes and changes in cell states, including (1) changes in stiffness of red blood cells in cytoskeletal disorders, such as malaria and sickle cell anemia [6, 7]; (2) increased cellular deformability of invasive cancer cells, compared with benign counterparts [8–10]; (3) increased stiffness of leukocytes in sepsis [11]; and (4) decreased deformability during the stem cell differentiation process [12–14].

In the following section, we discuss the well-established techniques that are being used to measure cellular mechanical properties, including atomic force microscopy (AFM) [15–24] and micropipette aspiration [25]. In addition, we describe the emerging microfluidic approaches (e.g., constriction channels, optical stretchers, hydrodynamic stretchers) for the characterization of cellular mechanical properties [26–29].

2 Cellular Mechanical Properties with Various Cell States

2.1 Red Blood Cell Disorders

Malaria is currently one of the world's most threatening diseases, infecting about 200 million people and leading to roughly 2,000 deaths per day [30, 31]. Malaria infection is caused by a single-cell parasite of the genome of *Plasmodium* [32]; after parasite invasion, red blood cells undergo extensive structural and molecular changes during a 48-h intra-erythrocytic cycle, leading to decreases in cellular deformability and increases in cellular adhesiveness [4, 5, 33]. The changes in the mechanical properties of red blood cells after *P. falciparum* infection have been probed using micropipette aspiration [34–36], optical tweezers [33, 37, 38], and microfluidic constriction channels [39–41]. The stiffness of red blood cells with the *P. falciparum* infection is approximately nine times that of their healthy counterparts [33]; the stiffer infected red blood cells were found to irreversibly block the passage of normal red blood cells when they were forced to travel through microfluidic constriction channels [39].

Sickle cell anemia is a hereditary blood disorder where changes in the molecular structure of hemoglobin result in stiffer sickle or crescent-shaped red blood cells, giving rise to circulation problems and depriving tissues and organs of oxygenated blood [42–45]. Studies of cell mechanics using, for example, micropipette aspiration [46–51], have been performed to probe the changes in mechanical properties of sickle-shaped red blood cells; red blood cells from sickle cell anemia patients are stiffer and more viscous when compared with the healthy red blood cells [52, 53].

2.2 Tumor

Cancer is currently one of the leading causes of death worldwide, with roughly 14 million new cases and more than 8 million deaths in 2012 [54]. Cancer is a disease that results from rapid, unrestricted, and uncontrolled proliferation of abnormal cells, due to dysregulation of the cellular signaling pathways that control cell proliferation and apoptosis—generally caused by mutations in genes that express key proteins involved in these biochemical reactions [55, 56].

Cancer is also accompanied by specific changes in the mechanical properties of cells [8, 10, 57], which have been probed using micropipette aspiration [58–62], AFM [63–90], magnetic twisting cytometry [91], microfluidic optical stretchers [92, 93], microfluidic constriction channels [94–97], and microfluidic hydrodynamic stretchers [98]. Experimental findings have revealed that cellular stiffness decreases significantly with malignant transformation in a variety of cancers, including breast cancer, lung cancer, renal cancer, prostate cancer, oral cancer, and skin cancer (see Table 1).

2.3 Leukocyte Activation in Sepsis

Sepsis is a progressive, injurious, inflammatory response to overwhelming infection associated with tissue hypoperfusion and multiorgan dysfunction [99, 100]. Neutrophils are crucial components of the innate immune response during sepsis, releasing important regulatory cytokines and contributing directly to antimicrobial killing. In patients with sepsis, reprogramming of neutrophil occurs, manifested by impaired recruitment of neutrophils to sites of infection, abnormal accumulation of neutrophils to remote sites, and dysregulation of neutrophil effector responses [11, 101, 102]. Changes in neutrophil rigidity and sequestration during sepsis have also been reported, leading to neutrophil accumulation in capillary beds, particularly in the lung and liver sinusoids. The changes in the mechanical properties of neutrophils have been probed using polymeric filters [101, 103], micropipette aspiration [104–106], and microfluidic constriction channels [107–109]. The results have confirmed that leukocyte deformability decreases in patients with sepsis, and that this change negatively affects the rheological properties of whole blood.

Table 1 Key developments in the field of mechanical phenotypes of tumor cells

Cell types	Techniques and quantified parameters	Key results
Normal rat embryo fibroblasts (CREF) and CREF transfected with T24 ras oncogene (CREF T24)	Micropipette aspiration + $E_{instantaneous}$ and $E_{equilibrium}$	The CREF T24 cells were 50 % more deformable than CREF cells [62]
Two normal cells of Hu609 and HCV29 and two bladder cancerous cells of T24 and BC3726	AFM + $E_{elastic}$ (elastic modulus)	Values of $E_{elastic}$ of Hu609, HCV29, T24, and BC3726 cells (ca. 20 cells per type) were 12.9 ± 4.8, 10.0 ± 4.6, 1.0 ± 0.5, and 1.4 ± 1.0 kPa, respectively [81]
Normal hepatocytes and hepatocellular carcinoma cells (HCC)	Micropipette aspiration + $E_{instantaneous}$ and $E_{equilibrium}$	Values of $E_{instantaneous}$ and $E_{equilibrium}$ of normal hepatocyptes (n = 24) were 181 ± 34 and 131 ± 18 Pa, respectively; for HCC (n = 30) they were 219 ± 34 and 155 ± 19 Pa, respectively [60]
Breast benign cell line of MCF-10; malignant tumor cells of MCF-7, mod-MCF-7, MDA-MB-231, and mod-MDA-MB-231	Microfluidic optical stretcher + optical deformability	Optical deformabilities of MCF-10 (n = 36), MCF-7 (n = 26), mod-MCF-7 (n = 21), MDA-MB-231, and mod-MDA-MB-231 cells were 10.5 ± 0.8, 21.4 ± 1.1, 30.4 ± 1.8, 33.7 ± 1.4, and 24.4 ± 2.5, respectively [93]
Human benign reactive mesothelial cells and metastatic tumor cells in human pleural fluid samples	AFM + $E_{elastic}$	Values of $E_{elastic}$ of tumor cells (n = 8 for each patient sample) and benign mesothelial cells (n = 8 for each patient sample) were 0.53 ± 0.10 and 1.97 ± 0.70 kPa, respectively [83]
Prostate tumor cell lines of LNCaP, PC-3, and BPH	AFM + $E_{elastic}$	Values of $E_{elastic}$ of LNCaP (n = 52), PC-3 (n = 53), and BPH cells (n = 47) were 287 ± 52, 1401 ± 162, and 2797 ± 491 Pa, respectively [87]
Breast benign cell line of MCF-10A and malignant tumor cells of MCF-7	AFM + $E_{elastic}$	MCF-7 cells had a value of $E_{elastic}$ significantly lower (1.4–1.8 times) than that of MCF-10A cells [88]
Breast benign cell line of MCF-10A and malignant tumor cells of MCF-7	Microfluidic constriction channel + entry time and transit velocity	MCF-10A cells had a longer entry time than MCF-7 cells, but a comparable transit velocity [97]

(continued)

Table 1 (continued)

Cell types	Techniques and quantified parameters	Key results
Breast tumor cell line of MCF-7 and cervical tumor cell line of HeLa	AFM + $E_{elastic}$	Values of $E_{elastic}$ of MCF-7 and HeLa cells (n > 15) were within the ranges 20–30 and 100–200 kPa, respectively [89]
Prostate tumor cell lines of LNCaP and PC-3	AFM + $E_{elastic}$	Values of $E_{elastic}$ of LNCaP and PC-3 were < 2.0 and 3.0–4.5 kPa, respectively [85]
Normal squamous, metaplastic, and dysplastic cell lines of EPC2, CP-A, and CP-D	AFM + $E_{elastic}$	Values of $E_{elastic}$ of EPC2 (n = 18), CP-A (n = 10), and CP-D (n = 19) cells were 4.7, 3.1, and 2.6 kPa, respectively [90]
Breast cell lines of MCF-10, MCF-7, and MDA-MB 231; lung cell lines of A431 and A125; skin cell lines of Te354.T and MeWo; colon cell lines of Hacat and SW480; cervical cell lines of Me180 and Ms751	AFM + $E_{elastic}$	Values of $E_{elastic}$ of MCF-10 (n = 22), MCF-7 (n = 25), MDA-MB 231 (n = 35), A431 (n = 26), A125 (n = 26), Te354.T (n = 23), MeWo (n = 24), Hacat (n = 23), SW480 (n = 23), Me180 (n = 23), and Ms751 (n = 23) were 478 ± 69, 425 ± 31, 341 ± 41, 374 ± 64, 265 ± 35, 352 ± 59, 319 ± 53, 384 ± 55, 466 ± 77, 540 ± 75, and 471 ± 53 Pa, respectively [77]
Ovarian surface epithelial (OSE) cells	AFM + $E_{elastic}$	Values of $E_{elastic}$ of early and late-stage OSE cells were 1.097 ± 0.632 and 0.549 ± 0.281 kPa, respectively [75]
Metastatic B16 melanoma variants, including B16-F10, B16-BL6, and B16-F1	AFM + $E_{elastic}$	Values of $E_{elastic}$ of B16-F10, B16-BL6, and B16-F1 cells were 350.8 ± 4.8, 661.9 ± 16.5, and 727.2 ± 13.0 Pa, respectively [72]
Ovarian cell lines of IOSE, HEY, HEY A8, OVCAR-3, and OVCAR-4	AFM + $E_{elastic}$	Values of $E_{elastic}$ of IOSE (n = 55), HEY (n = 60), HEY A8 (n = 59), OVCAR-3 (n = 20), and OVCAR-4 (n = 18) cells were 2.472 ± 2.048, 0.884 ± 0.529, 0.494 ± 0.222, 0.576 ± 0.236, and 1.120 ± 0.865 kPa, respectively [71]
Brain normal human glial cells, tumor cell lines of A172 and 1321N1	Microfluidic constriction channel + entry time and transit velocity	Brain tumor cells had shorter entry time than benign counterparts [95]

2.4 Stem Cell Differentiation

Stem cells have unique capacities to regenerate functional tissues continually for the lifetime of an organism [110, 111]. Realization of the potential of stem cells for tissue engineering requires characterization of their unique biological, biochemical, and proteomic properties, which have yet to be fully elucidated [112]. Changes in mechanical properties of cells have been reported during stem cell differentiation [13, 14], as probed using micropipette aspiration [113–115], AFM [116–120], and microfluidic hydrodynamic stretchers [98]. Significant decreases in cellular deformability have been observed for differentiated stem cells, compared with their undifferentiated counterparts (see Table 2).

Table 2 Key developments in the field of mechanical phenotypes of stem cells

Cell types	Techniques and quantified parameters	Key results
Human adipose–derived adult stem cells, bone marrow–derived mesenchymal stem cells, primary chondrocytes, and osteoblasts	AFM + $E_{instantaneous}$ and $E_{equilibrium}$	Values of $E_{instantaneous}$ and $E_{equilibrium}$ of osteoblasts (n = 43), chondrocytes (n = 50), adult stem cells (n = 52), and mesenchymal stem cells (n = 67) were 6.5 ± 2.7 and 4.5 ± 2.3 kPa, 1.8 ± 1.7 and 1.0 ± 1.6 kPa, 2.5 ± 1.2 and 1.7 ± 1.1 kPa, and 3.2 ± 2.2 and 2.3 ± 2.1 kPa, respectively [116]
Human bone marrow–derived mesenchymal stem cells	Micropipette aspiration + $E_{instantaneous}$ and $E_{equilibrium}$	Values of $E_{instantaneous}$ and $E_{equilibrium}$ of human mesenchymal stem cells were 518 ± 280 and 126 ± 81 Pa, respectively [113]
Human embryonic stem cells with chondrogenical differentiation; primary articular chondrocytes	Unconfined creep cytocompression + $E_{instantaneous}$ and $E_{equilibrium}$	Values of $E_{instantaneous}$ and $E_{equilibrium}$ of human embryonic stem cells (n > 10), chondrogenically differentiated human embryonic stem cells (n > 10), and articular chondrocytes (n > 10) were 0.53 ± 0.33 and 0.37 ± 0.20 kPa, 1.83 ± 0.75 and 1.09 ± 0.44 kPa, and 1.33 ± 0.37 and 1.14 ± 0.31 kPa, respectively [121]

(continued)

Table 2 (continued)

Cell types	Techniques and quantified parameters	Key results
Human mesenchymal stem cells with adipogenesis or osteogenesis	Micropipette aspiration + $E_{instantaneous}$ and $E_{equilibrium}$	Values of $E_{instantaneous}$ and $E_{equilibrium}$ of undifferentiated human mesenchymal stem cells, stem cells with adipogenesis, and stem cells with osteogenesis were 466 ± 87 and 116 ± 15 Pa, 420 ± 52 and 87 ± 23 Pa, and 890 ± 219 and 224 ± 40 Pa, respectively [114]
Undifferentiated and early differentiating mouse embryonic stem cells	AFM + $E_{elastic}$	Values of $E_{elastic}$ of undifferentiated (n > 10) and early differentiating mouse embryonic stem cells (n > 10) were 1.49 ± 0.09 and 16.07 ± 1.48 kPa, respectively, when using a pyramidal tip, and 0.2176 ± 0.015 and 0.4473 ± 0.036 kPa, respectively, when using a spherical tip [117]
Undifferentiated and early differentiating mouse and human embryonic stem cells	Microfluidic hydrodynamic stretcher + deformability	Deformabilities of undifferentiated (n = 3535) and early differentiating mouse embryonic stem cells (n = 1046) were 1.68 and 1.54, respectively; for undifferentiated (n = 2523) and early differentiating human embryonic stem cells (n = 2283), they were 1.82 and 1.59, respectively [98]
Human mesenchymal stem cells	AFM + $E_{elastic}$	Values of $E_{elastic}$ of mesenchymal stem cells (n > 10) were 15.4 ± 1.9 kPa for the cytoplasm and 11.9 ± 2.2 kPa for the nucleus portions [118]
Human amniotic fluid stem cells and murine osteoblast (OB6) cells	AFM + $E_{elastic}$	Values of $E_{elastic}$ of human amniotic fluid stem cells were 32.9 ± 3.66 kPa for the cytoskeleton and 13.9 ± 2.25 kPa for the nucleus portions; for OB6, they were 42.8 ± 3.44 and 26.9 ± 3.41 kPa, respectively [119]

(continued)

Table 2 (continued)

Cell types	Techniques and quantified parameters	Key results
Human adipose–derived stem cells	AFM + $E_{elastic}$	Values of $E_{elastic}$ of live (n > 10) and dead human adipose–derived stem cells (n > 10) were 1.27 and 18.61 kPa, respectively [120]
Bone marrow–derived human mesenchymal stem cells with differentiation toward smooth muscle cells	Micropipette aspiration + $E_{instantaneous}$ and $E_{equilibrium}$	Values of $E_{instantaneous}$ and $E_{equilibrium}$ of differentiating stem cells toward smooth muscle cells were 622.9 ± 114.2 and 144.3 ± 11.6 Pa, respectively—significantly higher than those values of undifferentiated stem cells [115]

3 Established Approaches for Quantifying Cellular Mechanical Properties

3.1 AFM

Because of increasing interest in the characterization of cellular mechanical properties, several approaches have been developed (Fig. 1) to quantify the intrinsic mechanical properties of individual cells [5, 122–124]. Among them, AFM has been proven to be a valuable tool for probing individual cellular surfaces at specific locations to measure the localized elasticity (Fig. 1a). Typically, a pyramidal or spherical probe tip attached to a flexible cantilever is pressed into the cellular surface for a set distance and then the deflection of the cantilever is measured using a laser beam, with mathematical models used to estimate the stiffness of the probed surface [15–24, 125].

Upon changing the external conditions, the change in elasticity of a cell membrane, quantified using AFM, is much greater than the change in the morphology of the cell, based on the following four factors [74, 88, 126, 127]. The first is the depth of indentation. For small indentation depths, histograms of the relative values of the Young's modulus describe regions rich in the network of actin filaments; for large indentation depths, however, the modulus represents the stiffness of the whole cell, typically accompanied by a decrease in its value (see Fig. 2a, b). The second factor is the effect of the substrate used for cell attachment, potentially leading to different Young's moduli for cells originating from the same tumor type (see Fig. 2c). The third parameter is the load rate, which can lead to significant differences in modulus after fitting with the Hertz model (see Fig. 2d). The fourth factor is linked to the

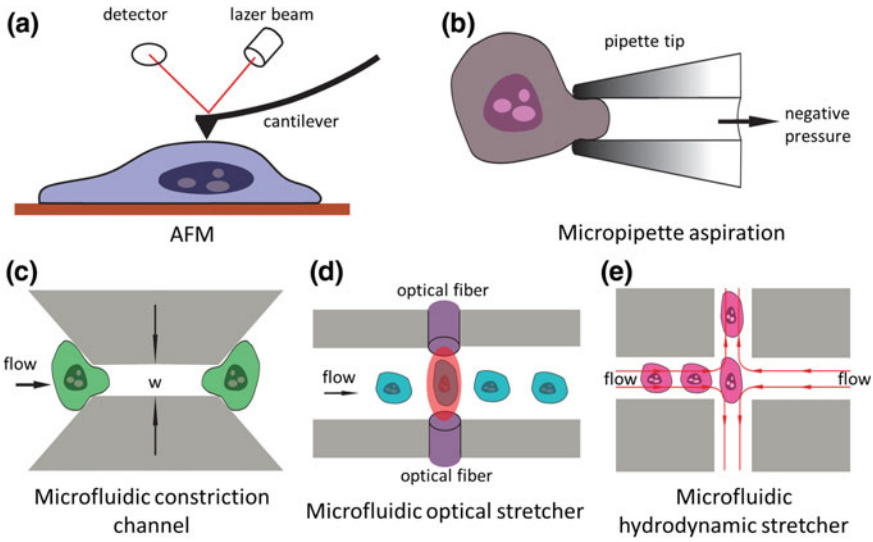

Fig. 1 Techniques enabling characterization of the mechanical properties of single cells. **a** AFM, where a sharp tip at the free end of a flexible cantilever generates a local deformation on the cell surface, an indicator of the cellular mechanical properties. **b** Micropipette aspiration, where a cell is deformed by applying suction through a micropipette placed on the surface of the cell to infer the cellular elastic responses, based on recorded geometrical changes. **c** A microfluidic constriction channel, where differences in hydraulic pressure squeeze cells through a channel having a small cross-sectional area, with the cell's transit time recorded as an indicator of its mechanical properties. **d** A microfluidic optical stretcher, where a two-beam laser trap is formed to serially deform single suspended cells, under optically induced surface forces, to measure mechanical properties of single cells. **e** A microfluidic hydrodynamic stretcher, where the cell under measurement is exposed to fluid stresses and the corresponding deformations are collected as stiffness indicators

position and time of the cell poking event, because the force curves, recorded at constant positions, usually manifest a narrow histogram that may not reflect the stiffness of a whole cell (see Fig. 2e, f).

3.2 Micropipette Aspiration

Micropipette aspiration is a well-established technique that enables determination of cellular mechanical properties through aspiration of the surface of a cell into a small glass tube with the leading edge of its surface tracked (see Fig. 1b). Interpretation of the measured data, using basic continuum models, leads to values for a cell's elastic and viscous properties. In particular, based on the equivalent model (e.g., a liquid surrounded by an elastic cortical shell), neutrophils were found to have a cortical surface tension of approximately 30 pN/μm and a viscosity on the order of 100 Pa s. On the other hand, chondrocytes and endothelial cells behave as homogeneous elastic solids with quantified elastic moduli on the order of 500 Pa [25].

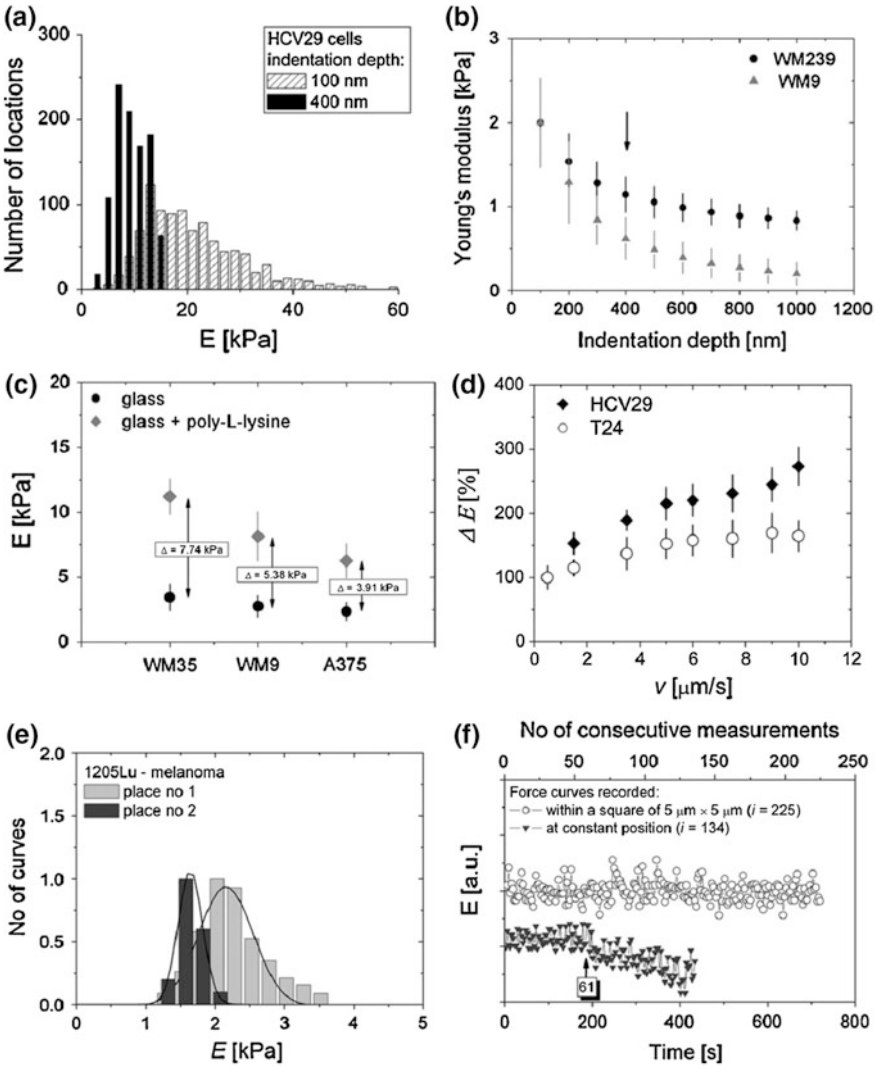

Fig. 2 Factors influencing the mechanical properties of single cells probed using AFM. **a** Young's moduli determined at tip indentation depths of 100 and 400 nm (nonmalignant HCV29 bladder cell). **b** Young's moduli determined as a function of tip indentation depth [human melanoma cell lines: WM239 (skin) and WM9 (lymph node metastasis)]. **c** Influence of surface properties on Young's modulus, quantified using AFM (WM35-primary melanoma, and two metastatic cell lines: WM9 and A375). **d** Changes in Young's modulus as a function of the tip scanning rate (nonmalignant and malignant human bladder cells). **e** Effect of the relative positions of cell poking on cellular Young's modulus (melanoma 1205Lu). **f** Effect of repeated cell poking on the quantification of Young's modulus (nonmalignant and malignant human bladder cells). Reproduced with permission from ref. [74]. Copyright 2012, Elsevier Ltd

Compared with AFM, micropipette aspiration deforms a cell in a more global manner, leading to more accurate characterization of cellular mechanical properties. Although precise, this technique requires skilled manual operation and proceeds with very low throughput (<1 cell/10 min) [4]. To address this issue, an automated micropipette aspiration setup was recently proposed where a micromanipulator, a motorized translation stage, and a custom-built pressure system to position a micropipette were controlled with real-time visual feedback to accurately measure cell deformations online. This system still suffers, however, from the issue of low throughput, with the mechanical properties reported from only approximately 30 cells for each cell type [128, 129].

4 Emerging Microfluidic Tools for Characterization of Cellular Mechanical Properties

Microfluidics is a science and technology related to the processing and manipulation of small volumes of fluids (from 10^{-9} to 10^{-18} l) in channels having dimensions on the scale of tens of micrometers [130–132]. The micrometer-scale dimensions of the devices match well with the size of a typical biological cell, making microfluidics an ideal platform for cell studies [133–137]. More specifically, microfluidics has been used for characterizing biochemical (e.g., gene and protein) and/or biophysical (mechanical and electrical) properties of cells at the single-cell level [138–144].

In the field of microfluidics-based characterization of cellular mechanical properties, three major approaches have been developed so far [26–29]: microfluidic constriction channels [39–41, 94–97, 145–162] (see Fig. 1d), microfluidic optical stretchers [92, 93, 163, 164] (see Fig. 1e), and microfluidic hydrodynamic stretchers [98] (see Fig. 1f). Compared with conventional techniques, these microfluidic approaches display significantly higher throughput, enabling the collection of data from large numbers of cells.

4.1 Microfluidic Constriction Channel

The microfluidic constriction channel is designed to operate by evaluating the transition process as cells pass through microchannels having cross-sectional areas smaller than the dimensions of a single cell (see Fig. 3). An attractive feature of this technique is the ability to achieve higher throughput than those of conventional approaches (e.g., micropipette aspiration) for cellular mechanical characterization (up to ca. 1 cell/s). This technique was first used to evaluate the mechanical properties of red blood cells [39–41, 145–152, 165], and then further expanded to study the deformability of white blood cells [153] and tumor cells [94–97, 154].

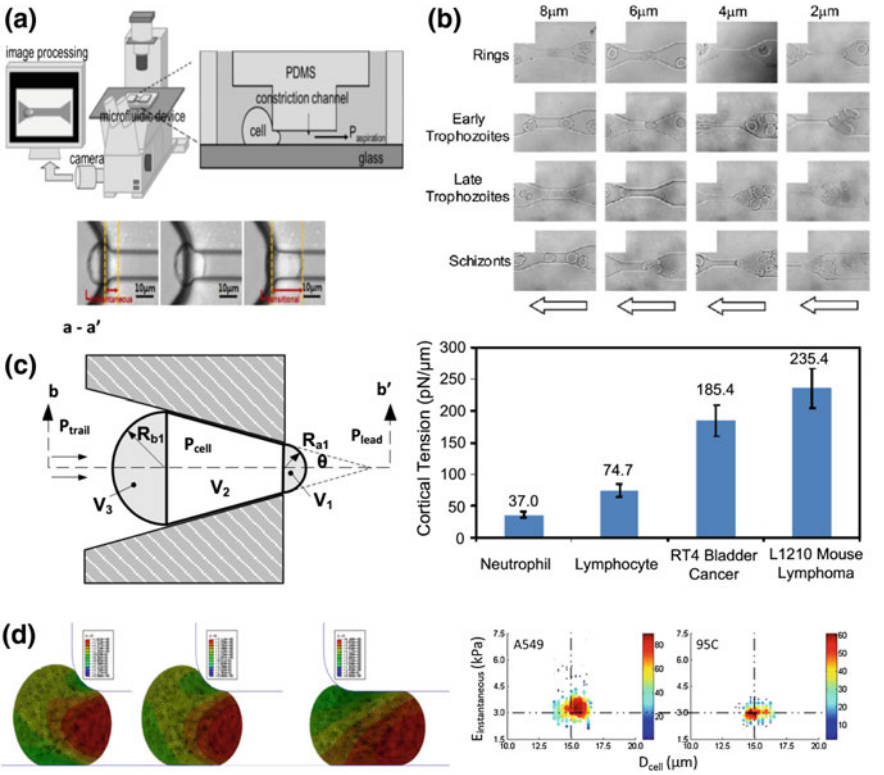

Fig. 3 Experimental setup and key application results of microfluidic constriction channels used for the characterization of cellular mechanical properties. **a** Schematic and raw experimental images of a microfluidic constriction channel for the characterization of cellular mechanical properties, where hydraulic pressure differences squeeze cells through a channel having a small cross-sectional area, with the cell transit time recorded as an indicator of the mechanical properties. Reproduced with permission from ref. [157]. Copyright 2014, Elsevier Ltd. **b** Four sequences of video images recorded during four stages of malaria-infected red blood cells (early ring stage, early trophozoite, late trophozoite, schizont) passing through constriction channels. Ring-stage-infected erythrocytes retained much of the structural characteristics of normal erythrocytes and could pass through all constricted channels. Early trophozoite and late trophozoite-infected cells passed through the larger (8 and 6 μm) channels, but eventually blocked the smaller (4 and 2 μm) channels. Schizont-stage-infected erythrocytes blocked all but the 8 μm channel. The arrows indicate the direction of flow. Reproduced with permission from ref. [39]. Copyright 2003, the National Academy of Sciences of the USA. **c** Models of the cellular entry process into the constriction channel, enabling quantification of the cortical tensions of blood cells and tumor. Reproduced with permission from ref. [158]. Copyright 2012, Royal Society of Chemistry. **d** Numerical simulations of the cellular entry process into the constriction channel, using a cellular viscoelastic model, rather than a liquid droplet model, and taking cellular friction with constriction channel walls into consideration, enabling quantification of the instantaneous Young's moduli of single cells. Reproduced with permission from ref. [157]. Copyright 2014, Elsevier Ltd

Initially, the cellular entry time and transit velocity through the constriction channel were used as biophysical markers to evaluate the cellular mechanical properties. These parameters cannot reflect the intrinsic cellular mechanical properties because they are highly dependent on the cellular sizes. To tackle this issue, several groups have modeled the cellular entry process into the constriction channel, with the purpose of translating cell-dependent mechanical biomarkers into size-independent parameters [155–159].

Lim et al. modeled the cellular entry process into the constriction channel using numerical simulations, suggesting that the cell entry time depends strongly on the cortical stiffness [159]. Ma et al. simplified the cellular entry process and quantified the cortical tension of blood and tumor cells as the first reported use of the constriction channel design to characterize size-independent mechanical properties [158, 160]. Chen et al. used numerical simulations to model the cellular entry process into the constriction channel, employing a cellular viscoelastic model, rather than a liquid droplet model, thereby enabling the quantification of the instantaneous Young's moduli of single cells [157]. In addition, because small constriction channels are prone to clogging, constriction channels with adjustable cross-sectional areas have also been proposed to address the clogging issue to a certain extent [161, 162].

4.2 Microfluidic Optical Stretcher

In an optical stretcher, a two-beam laser trap is used to serially deform single suspended cells, through optically induced surface forces, and, thereby, measure the mechanical properties of single cells (see Fig. 4). This technique has been integrated with microfluidic channels and operates on spherically symmetrical cells in suspension [92, 93, 163, 164]. It was first used to classify MCF-10, MCF-7, and mod-MCF-7 cells, revealing a fivefold increase in deformability for cancer cells relative to benign counterparts [92, 93].

Furthermore, the microfluidic optical stretcher has been used to quantify acute leukemia cells during differentiation therapy, revealing significant softening of neutrophils during the differentiation process [163]. In addition, the compliance of cells from cell lines and primary samples of healthy donors and cancer patients has been measured using the microfluidic optical stretcher, revealing that cancer cells were 3.5 times more compliant than cells from healthy donors [164].

The microfluidic optical stretcher does, however, have two significant limitations. First, its throughput remains at approximately 1 cell/min, and it cannot be improved significantly. This limitation is due to the trade-off between higher optical forces and increased optical power leading to significant heating of the measured cells. Second, the quantified cellular deformability is not an intrinsic biomechanical marker because it depends on the cellular size and the characterization conditions.

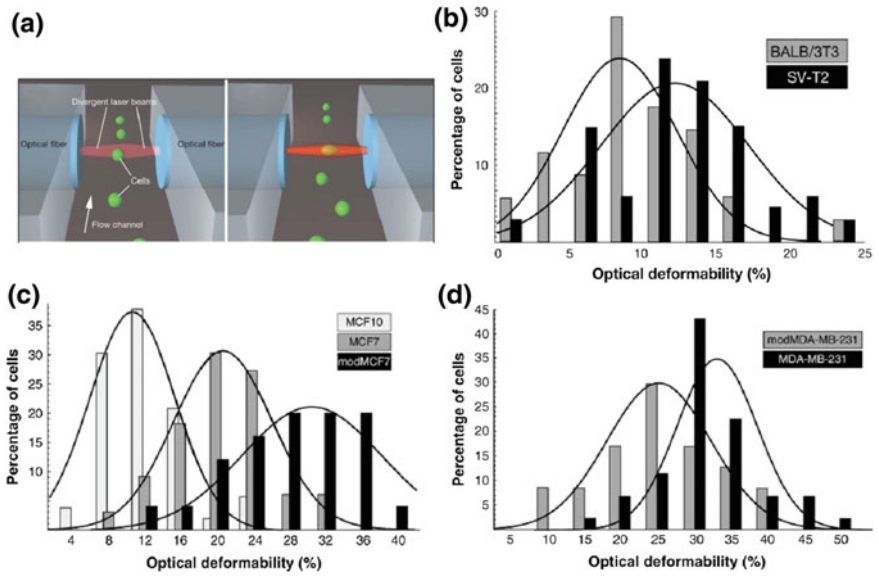

Fig. 4 Experimental setup of and key results from microfluidic optical stretchers used for the characterization of cellular mechanical properties. **a** Schematic representation of a microfluidic optical stretcher; a two-beam laser trap is used to serially deform a single suspended cell, through optically induced surface forces, to measure the mechanical properties of the cell. **b** The optical deformability of malignantly transformed SV-T2 fibroblasts is significantly higher than that of normal BALB/3T3 fibroblasts ($OD_{BALB/3T3}$ = 8.4 ± 1.0; $OD_{SV\text{-}T2}$ = 11.7 ± 1.1). **c** Optical deformabilities of three populations of MCF cell lines: $OD_{MCF\text{-}10}$ = 10.5 ± 0.8; $OD_{MCF\text{-}7}$ = 21.4 ± 1.1; $OD_{modMCF\text{-}7}$ = 30.4 ± 1.8. **d** Two populations of MDA-MB-231 cell lines are clearly distinguishable in the histograms of the measured optical deformability ($OD_{MDA\text{-}MB\text{-}231}$ = 33.7 ± 1.4; $OD_{modMDA\text{-}MB\text{-}231}$ = 24. 4 ± 2.5). Reproduced with permission from ref. [93]. Copyright 2005, Biophysical Society

4.3 Microfluidic Hydrodynamic Stretcher

In a microfluidic hydrodynamic stretcher, fluid stresses are generated by elaborately designing channel geometries, which are used to deform single cells. The rigidity of RBCs has been investigated using shear flow in narrowing channels [166] and extensional flow in hyperbolic converging channels [167]. Recently, inertial focusing is used to deliver cells uniformly to a stretching extensional flow, where cells are deformed at high strain rates, while a high-speed camera records images that can be used to extract biophysical parameters (see Fig. 5) [98]. Unlike the techniques discussed above, this approach is capable of ultrahigh throughput (ca. 1000 cells/s). It has been used to quantify native populations of leukocytes and malignant cells in pleural effusions; the experimental deformability data can be used to predict disease states in patients with cancer or immune activation, with a sensitivity of 91 % and a specificity of 86 %.

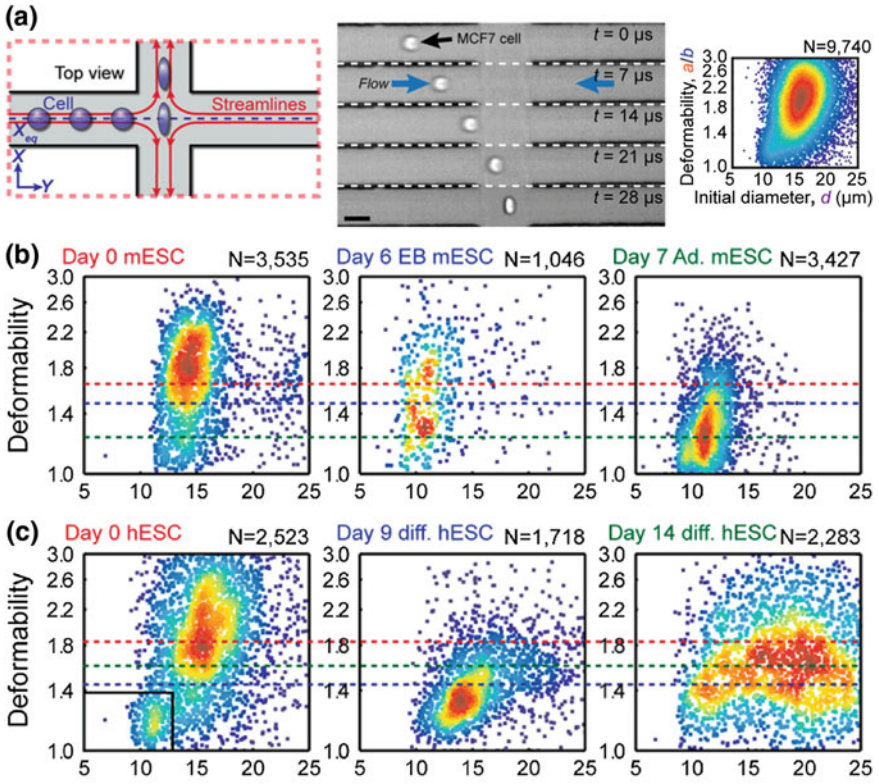

Fig. 5 Experimental setup of and key results from microfluidic hydrodynamic stretchers used for characterization of cellular mechanical properties. **a** Schematic representation, raw experimental images, and quantified deformability of the microfluidic hydrodynamic stretcher for characterization of cellular mechanical properties, where single cells under measurement are exposed to fluid stresses and the corresponding deformations are collected as stiffness indicators. **b**, **c** Decreased deformability has been correlated with increased stem cell pluripotency for **b** mouse embryonic stem cells and **c** human embryonic stem cells. Reproduced with permission from ref. [98]. Copyright 2012, the National Academy of Sciences of the USA

5 Conclusion

Various proof-of-concept approaches have been developed for the characterization of the mechanical properties of single cells, enabling correlations to be made between cellular mechanical properties and cellular biophysical statuses. Nevertheless, to convince the wider cell biology and clinical communities of the merits of cellular biophysical biomarkers, much research effort remains to be exerted in the development of both equipment and applications.

For conventional approaches (e.g., AFM and micropipette aspiration) capable of collecting size-independent intrinsic biophysical markers (e.g., instantaneous and

equilibrium Young's moduli), the issue of low throughout (ca. 1 cell per 10 min) without the capability of collecting statistically significant data remains problematic. For microfluidic approaches enabling high-throughput characterization of the biomechanical properties of single cells (ca. 1000 cells/s), the collected parameters remain dependent on the cell size and experimental conditions (e.g., pressure drop, channel geometry). Thus, further technical developments remain necessary to enable characterization of the intrinsic biophysical properties of single cells in a high-throughput manner.

Furthermore, the correlations between biophysical markers and the biochemical properties of single cells should be explored further. It is possible to design experiments to characterize both cellular biophysical (e.g., Young's modulus) and biochemical markers, including genetic and protein information, simultaneously, potentially revealing correlations between these biophysical and biochemical markers. This process should also provide a comprehensive understanding of cellular status at the single-cell level, paving the foundation for further studies of cell biology.

Acknowledgment We thank the National Basic Research Program of China (973 Program, Grant No. 2014CB744600), the National Natural Science Foundation of China (Grant Nos. 61201077, 61431019 and 81261120561), the National High Technology Research and Development Program of China (863 Program, Grant No. 2014AA093408), and the Beijing NOVA Program of Science and Technology for financial support.

References

1. Ethier CR, Simmons CA (2007) Introductory biomechanics: from cells to organisms. Cambridge texts in biomedical engineering, vol xiii. Cambridge University Press, Cambridge, 511 p, [16] p. of plates
2. Fletcher DA, Mullins RD (2010) Cell mechanics and the cytoskeleton. Nature 463 (7280):485–492
3. Lim CT, Zhou EH, Quek ST (2006) Mechanical models for living cells—a review. J Biomech 39(2):195–216
4. Di Carlo D (2012) A mechanical biomarker of cell state in medicine. J Lab Autom 17(1):32–42
5. Lee GYH, Lim CT (2007) Biomechanics approaches to studying human diseases. Trends Biotechnol 25(3):111–118
6. Diez-Silva M et al (2010) Shape and biomechanical characteristics of human red blood cells in health and disease. MRS Bull 35(5):382–388
7. Lim CT, Li A (2011) Mechanopathology of red blood cell diseases—Why mechanics matters. Theor Appl Mech Lett 1(1):014000
8. Suresh S (2007) Biomechanics and biophysics of cancer cells. Acta Biomater 3(4):413–438
9. Katira P, Bonnecaze RT, Zaman MH (2013) Modeling the mechanics of cancer: effect of changes in cellular and extra-cellular mechanical properties. Front Oncol 3:145
10. Zhang W et al (2013) A brief review of the biophysical hallmarks of metastatic cancer cells. Cancer Hallm 1(2–3):59–66
11. Kovach MA, Standiford TJ (2012) The function of neutrophils in sepsis. Curr Opin Infect Dis 25(3):321–327

12. Keefer CL, Desai JP (2011) Mechanical phenotyping of stem cells. Theriogenology 75 (8):1426–1430
13. Li D et al (2011) Role of mechanical factors in fate decisions of stem cells. Regenerative Med 6(2):229–240
14. Discher DE, Mooney DJ, Zandstra PW (2009) Growth factors, matrices, and forces combine and control stem cells. Science 324(5935):1673–1677
15. Lehenkari PP et al (2000) Adapting atomic force microscopy for cell biology. Ultramicroscopy 82(1–4):289–295
16. Charras GT, Horton MA (2002) Single cell mechanotransduction and its modulation analyzed by atomic force microscope indentation. Biophys J 82(6):2970–2981
17. Radmacher M (2002) Measuring the elastic properties of living cells by the atomic force microscope. Methods Cell Biol 68:67–90
18. Alonso JL, Goldmann WH (2003) Feeling the forces: atomic force microscopy in cell biology. Life Sci 72(23):2553–2560
19. Costa KD (2003) Single-cell elastography: probing for disease with the atomic force microscope. Dis Markers 19(2–3):139–154
20. Costa KD (2006) Imaging and probing cell mechanical properties with the atomic force microscope. Methods Mol Biol 319:331–361
21. Kuznetsova TG et al (2007) Atomic force microscopy probing of cell elasticity. Micron 38 (8):824–833
22. Lekka M, Laidler P (2009) Applicability of AFM in cancer detection. Nat Nanotechnol 4 (2):72
23. Kirmizis D, Logothetidis S (2010) Atomic force microscopy probing in the measurement of cell mechanics. Int J Nanomed 5:137–145
24. Shi X et al (2012) Living cell study at the single-molecule and single-cell levels by atomic force microscopy. Nanomedicine 7(10):1625–1637
25. Hochmuth RM (2000) Micropipette aspiration of living cells. J Biomech 33(1):15–22
26. Kim DH et al (2009) Microengineered platforms for cell mechanobiology. Annu Rev Biomed Eng 11:203–233
27. Zheng Y, Sun Y (2011) Microfluidic devices for mechanical characterisation of single cells in suspension. Micro Nano Lett 6(5):327–331
28. Mao X, Huang TJ (2012) Exploiting mechanical biomarkers in microfluidics. Lab Chip 12 (20):4006–4009
29. Zheng Y et al (2013) Recent advances in microfluidic techniques for single-cell biophysical characterization. Lab Chip 13(13):2464–2483
30. White NJ et al (2014) Malaria. Lancet 383(9918):723–735
31. Grayson M (2012) Malaria. Nature 484(7395):1
32. Miller LH et al (2002) The pathogenic basis of malaria. Nature 415(6872):673–679
33. Suresh S et al (2005) Connections between single-cell biomechanics and human disease states: gastrointestinal cancer and malaria. Acta Biomater 1(1):15–30
34. Nash GB et al (1989) Abnormalities in the mechanical properties of red blood cells caused by Plasmodium falciparum. Blood 74(2):855–861
35. Paulitschke M, Nash GB (1993) Membrane rigidity of red blood cells parasitized by different strains of Plasmodium falciparum. J Lab Clin Med 122(5):581–589
36. Glenister FK et al (2002) Contribution of parasite proteins to altered mechanical properties of malaria-infected red blood cells. Blood 99(3):1060–1063
37. Mills JP et al (2004) Nonlinear elastic and viscoelastic deformation of the human red blood cell with optical tweezers. Mech Chem Biosyst 1(3):169–180
38. Bambardekar K et al (2008) Measuring erythrocyte deformability with fluorescence, fluid forces, and optical trapping. J Biomed Opt 13(6):064021
39. Shelby JP et al (2003) A microfluidic model for single-cell capillary obstruction by Plasmodium falciparum infected erythrocytes. Proc Natl Acad Sci USA 100(25):14618–14622

40. Handayani S et al (2009) High deformability of Plasmodium vivax-infected red blood cells under microfluidic conditions. J Infect Dis 199(3):445–450
41. Bow H et al (2011) A microfabricated deformability-based flow cytometer with application to malaria. Lab Chip 11(6):1065–1073
42. Rees DC, Williams TN, Gladwin MT (2010) Sickle-cell disease. Lancet 376(9757):2018–2031
43. Cancado RD (2012) Sickle cell disease: looking back but towards the future. Rev Bras Hematol Hemoter 34(3):175–177
44. Darlison MW, Modell B (2013) Sickle-cell disorders: limits of descriptive epidemiology. Lancet 381(9861):98–99
45. Fottrell E, Osrin D (2013) Sickle cell anaemia in a changing world. PLoS Med 10(7): e1001483
46. Evans E, Mohandas N, Leung A (1984) Static and dynamic rigidities of normal and sickle erythrocytes. Major influence of cell hemoglobin concentration. J Clin Invest 73(2):477–488
47. Nash GB, Johnson CS, Meiselman HJ (1984) Mechanical properties of oxygenated red blood cells in sickle cell (HbSS) disease. Blood 63(1):73–82
48. Nash GB, Johnson CS, Meiselman HJ (1986) Influence of oxygen tension on the viscoelastic behavior of red blood cells in sickle cell disease. Blood 67(1):110–118
49. Evans EA, Mohandas N (1987) Membrane-associated sickle hemoglobin: a major determinant of sickle erythrocyte rigidity. Blood 70(5):1443–1449
50. Itoh T, Chien S, Usami S (1992) Deformability measurements on individual sickle cells using a new system with pO2 and temperature control. Blood 79(8):2141–2147
51. Itoh T, Chien S, Usami S (1995) Effects of hemoglobin concentration on deformability of individual sickle cells after deoxygenation. Blood 85(8):2245–2253
52. Barabino GA, Platt MO, Kaul DK (2010) Sickle cell biomechanics. Annu Rev Biomed Eng 12:345–367
53. Ballas SK, Mohandas N (2004) Sickle red cell microrheology and sickle blood rheology. Microcirculation 11(2):209–225
54. Ferlay J et al (2015) Cancer incidence and mortality worldwide: Sources, methods and major patterns in GLOBOCAN 2012. Int J Cancer 136(5):E359–E386
55. Ruddon RW (2007) Cancer biology, vol xiv, 4th ed. Oxford University Press, New York, 530 p
56. Weinberg RA (2007) The biology of cancer. Garland Science, Taylor and Francis, New York, London
57. Jonietz E (2012) Mechanics: the forces of cancer. Nature 491(7425):S56–S57
58. Ward KA et al (1991) Viscoelastic properties of transformed cells: role in tumor cell progression and metastasis formation. Biorheology 28(3–4):301–313
59. Thoumine O, Ott A (1997) Comparison of the mechanical properties of normal and transformed fibroblasts. Biorheology 34(4–5):309–326
60. Wu ZZ et al (2000) Comparison of the viscoelastic properties of normal hepatocytes and hepatocellular carcinoma cells under cytoskeletal perturbation. Biorheology 37(4):279–290
61. Zhang G et al (2002) Mechanical properties of hepatocellular carcinoma cells. World J Gastroenterol 8(2):243–246
62. Anderson K et al (1991) In vitro studies of deformation and adhesion properties of transformed cells. Cell Biophys 18(2):81–97
63. Saab MB et al (2013) Differential effect of curcumin on the nanomechanics of normal and cancerous Mammalian epithelial cells. Cell Biochem Biophys 65(3):399–411
64. Sarna M et al (2013) Nanomechanical analysis of pigmented human melanoma cells. Pigm Cell Melanoma Res 26(5):727–730
65. Andolfi L et al (2014) Investigation of adhesion and mechanical properties of human glioma cells by single cell force spectroscopy and atomic force microscopy. PLoS One 9(11): e112582
66. Liu H et al (2014) Biophysical characterization of bladder cancer cells with different metastatic potential. Cell Biochem Biophys 68(2):241–246

67. Omidvar R et al (2014) Atomic force microscope-based single cell force spectroscopy of breast cancer cell lines: an approach for evaluating cellular invasion. J Biomech 47 (13):3373–3379
68. Osmulski P et al (2014) Nanomechanical biomarkers of single circulating tumor cells for detection of castration resistant prostate cancer. Prostate 74(13):1297–1307
69. Ramos JR et al (2014) The softening of human bladder cancer cells happens at an early stage of the malignancy process. Beilstein J Nanotechnol 5:447–457
70. Rother J et al (2014) Atomic force microscopy-based microrheology reveals significant differences in the viscoelastic response between malign and benign cell lines. Open Biology 4(5):140046
71. Xu W et al (2012) Cell stiffness is a biomarker of the metastatic potential of ovarian cancer cells. PLoS One 7(10):e46609
72. Watanabe T et al (2012) Higher cell stiffness indicating lower metastatic potential in B16 melanoma cell variants and in (−)-epigallocatechin gallate-treated cells. J Cancer Res Clin Oncol 138:859–866
73. Plodinec M et al (2012) The nanomechanical signature of breast cancer. Nat Nanotechnol 7 (11):757–765
74. Lekka M et al (2012) Cancer cell recognition–mechanical phenotype. Micron 43(12):1259–1266
75. Ketene AN et al (2012) The effects of cancer progression on the viscoelasticity of ovarian cell cytoskeleton structures. Nanomedicine 8(1):93–102
76. Bastatas L et al (2012) AFM nano-mechanics and calcium dynamics of prostate cancer cells with distinct metastatic potential. Biochim Biophys Acta 1820(7):1111–1120
77. Jonas O, Mierke CT, Kas JA (2011) Invasive cancer cell lines exhibit biomechanical properties that are distinct from their noninvasive counterparts. Soft Matter 7(24):11488–11495
78. Cross SE et al (2011) Green tea extract selectively targets nanomechanics of live metastatic cancer cells. Nanotechnology 22(21):215101
79. Wang J et al (2009) Atomic force microscope study of tumor cell membranes following treatment with anti-cancer drugs. Biosens Bioelectron 25(4):721–727
80. Iyer S et al (2009) Atomic force microscopy detects differences in the surface brush of normal and cancerous cells. Nat Nanotechnol 4(6):389–393
81. Lekka M et al (1999) Elasticity of normal and cancerous human bladder cells studied by scanning force microscopy. Eur Biophys J 28(4):312–316
82. Lekka M et al (2001) The effect of chitosan on stiffness and glycolytic activity of human bladder cells. Biochim Biophys Acta 1540(2):127–136
83. Cross SE et al (2007) Nanomechanical analysis of cells from cancer patients. Nat Nanotechnol 2(12):780–783
84. Cross SE et al (2008) AFM-based analysis of human metastatic cancer cells. Nanotechnology 19(38):384003
85. Docheva D et al (2010) Effect of collagen I and fibronectin on the adhesion, elasticity and cytoskeletal organization of prostate cancer cells. Biochem Biophys Res Commun 402 (2):361–366
86. Tang X et al (2014) A mechanically-induced colon cancer cell population shows increased metastatic potential. Molecular Cancer 13:131
87. Faria EC et al (2008) Measurement of elastic properties of prostate cancer cells using AFM. Analyst 133(11):1498–1500
88. Li QS et al (2008) AFM indentation study of breast cancer cells. Biochem Biophys Res Commun 374(4):609–613
89. Leporatti S et al (2009) Cytomechanical and topological investigation of MCF-7 cells by scanning force microscopy. Nanotechnology 20(5):055103
90. Fuhrmann A et al (2011) AFM stiffness nanotomography of normal, metaplastic and dysplastic human esophageal cells. Phys Biol 8(1):015007

91. Coughlin MF et al (2013) Cytoskeletal stiffness, friction, and fluidity of cancer cell lines with different metastatic potential. Clin Exp Metastas 30(3):237–250
92. Lincoln B et al (2004) Deformability-based flow cytometry. Cytometry Part A 59A(2):203–209
93. Guck J et al (2005) Optical deformability as an inherent cell marker for testing malignant transformation and metastatic competence. Biophys J 88(5):3689–3698
94. Mak M, Erickson D (2013) A serial micropipette microfluidic device with applications to cancer cell repeated deformation studies. Integr Biology 5(11):1374–1384
95. Khan ZS, Vanapalli SA (2013) Probing the mechanical properties of brain cancer cells using a microfluidic cell squeezer device. Biomicrofluidics 7(1):11806
96. Byun S et al (2013) Characterizing deformability and surface friction of cancer cells. Proc Natl Acad Sci 110(19):7580–7585
97. Hou HW et al (2009) Deformability study of breast cancer cells using microfluidics. Biomed Microdevices 11(3):557–564
98. Gossett DR et al (2012) Hydrodynamic stretching of single cells for large population mechanical phenotyping. Proc Natl Acad Sci USA 109(20):7630–7635
99. Hotchkiss RS, Karl IE (2003) The pathophysiology and treatment of sepsis. N Engl J Med 348(2):138–150
100. Bone RC (1991) The pathogenesis of sepsis. Ann Intern Med 115(6):457–469
101. Yodice PC et al (1997) Neutrophil rheologic changes in septic shock. Am J Respir Crit Care Med 155(1):38–42
102. Alves-Filho JC et al (2008) The role of neutrophils in severe sepsis. Shock 30(Suppl 1):3–9
103. Worthen GS et al (1989) Mechanics of stimulated neutrophils: cell stiffening induces retention in capillaries. Science 245(4914):183–186
104. Poschl JM, Ruef P, Linderkamp O (2005) Deformability of passive and activated neutrophils in children with Gram-negative septicemia. Scand J Clin Lab Invest 65(4):333–339
105. Skoutelis AT et al (2000) Neutrophil deformability in patients with sepsis, septic shock, and adult respiratory distress syndrome. Crit Care Med 28(7):2355–2359
106. Linderkamp O et al (1998) Passive deformability of mature, immature, and active neutrophils in healthy and septicemic neonates. Pediatr Res 44(6):946–950
107. Inoue Y et al (2006) A neutrophil elastase inhibitor, sivelestat, improves leukocyte deformability in patients with acute lung injury. J Trauma 60(5):936–943
108. Nishino M et al (2005) Serial changes in leukocyte deformability and whole blood rheology in patients with sepsis or trauma. J Trauma 59(6):1425–1431
109. Tanaka H et al (2001) Granulocyte colony-stimulating factor (G-CSF) stiffens leukocytes but attenuates inflammatory response without lung injury in septic patients. J Trauma 51 (6):1110–1116
110. Lovell-Badge R (2001) The future for stem cell research. Nature 414(6859):88–91
111. Krupalnik V, Hanna JH (2014) Stem cells: The quest for the perfect reprogrammed cell. Nature 511(7508):160–162
112. Chamberlain JS (2006) Stem-cell biology: a move in the right direction. Nature 444 (7119):552–553
113. Tan SC et al (2008) Viscoelastic behaviour of human mesenchymal stem cells. BMC Cell Biology 9:40
114. Yu H et al (2010) Mechanical behavior of human mesenchymal stem cells during adipogenic and osteogenic differentiation. Biochem Biophys Res Commun 393(1):150–155
115. Khani MM et al (2014) Evaluation of mechanical properties of human mesenchymal stem cells during differentiation to smooth muscle cells. Ann Biomed Eng 42(7):1373–1380
116. Darling EM et al (2008) Viscoelastic properties of human mesenchymally-derived stem cells and primary osteoblasts, chondrocytes, and adipocytes. J Biomech 41(2):454–464
117. Pillarisetti A et al (2011) Mechanical phenotyping of mouse embryonic stem cells: increase in stiffness with differentiation. Cell Reprogram 13(4):371–380
118. Ruiz JP et al (2012) The effect of nicotine on the mechanical properties of mesenchymal stem cells. Cell Health Cytoskelet 4:29–35

119. Aryaei A, Jayasuriya AC (2013) Mechanical properties of human amniotic fluid stem cells using nanoindentation. J Biomech 46(9):1524–1530
120. Hu K, Zhao F, Wang Q (2013) Mechanical characterization of living and dead undifferentiated human adipose-derived stem cells by using atomic force microscopy. Proc Inst Mech Eng [H]: J Eng Med 227(12):1319–1323
121. Ofek G et al (2009) Mechanical characterization of differentiated human embryonic stem cells. J Biomech Eng 131(6):061011
122. Van Vliet KJ, Bao G, Suresh S (2003) The biomechanics toolbox: experimental approaches for living cells and biomolecules. Acta Mater 51(19):5881–5905
123. Lim CT et al (2006) Experimental techniques for single cell and single molecule biomechanics. Mater Sci Eng, C 26(8):1278–1288
124. Addae-Mensah KA, Wikswo JP (2008) Measurement techniques for cellular biomechanics in vitro. Exp Biol Med 233(7):792–809
125. Guo Q et al (2012) Characterization of cell elasticity correlated with cell morphology by atomic force microscope. J Biomech 45(2):304–309
126. Pogoda K et al (2012) Depth-sensing analysis of cytoskeleton organization based on AFM data. Eur Biophys J 41(1):79–87
127. Lekka M et al (2012) Cancer cell detection in tissue sections using AFM. Arch Biochem Biophys 518(2):151–156
128. Shojaei-Baghini E et al (2013) Mechanical characterization of benign and malignant urothelial cells from voided urine. Appl Phys Lett 102(12):123704
129. Shojaei-Baghini E, Zheng Y, Sun Y (2013) Automated micropipette aspiration of single cells. Ann Biomed Eng 41(6):1208–1216
130. Wootton RC, Demello AJ (2010) Microfluidics: exploiting elephants in the room. Nature 464 (7290):839–840
131. Whitesides GM (2006) The origins and the future of microfluidics. Nature 442(7101):368–373
132. Squires TM, Quake SR (2005) Microfluidics: fluid physics at the nanoliter scale. Rev Mod Phys 77(3):977
133. Sackmann EK, Fulton AL, Beebe DJ (2014) The present and future role of microfluidics in biomedical research. Nature 507(7491):181–189
134. El-Ali J, Sorger PK, Jensen KF (2006) Cells on chips. Nature 442(7101):403–411
135. Meyvantsson I, Beebe DJ (2008) Cell culture models in microfluidic systems. Annu Rev Anal Chem 1:423–449
136. Paguirigan AL, Beebe DJ (2008) Microfluidics meet cell biology: bridging the gap by validation and application of microscale techniques for cell biological assays. BioEssays 30 (9):811–821
137. Velve-Casquillas G et al (2010) Microfluidic tools for cell biological research. Nano Today 5(1):28–47
138. Thompson AM et al (2014) Microfluidics for single-cell genetic analysis. Lab Chip 14(17):3135–3142
139. Yin H, Marshall D (2012) Microfluidics for single cell analysis. Curr Opin Biotechnol 23(1):110–119
140. Lecault V et al (2012) Microfluidic single cell analysis: from promise to practice. Curr Opin Chem Biol 16(3–4):381–390
141. Ryan D, Ren K, Wu H (2011) Single-cell assays. Biomicrofluidics 5(2):21501
142. Zare RN, Kim S (2010) Microfluidic platforms for single-cell analysis. Annu Rev Biomed Eng 12:187–201
143. Sims CE, Allbritton NL (2007) Analysis of single mammalian cells on-chip. Lab Chip 7(4):423–440
144. Di Carlo D, Lee LP (2006) Dynamic single-cell analysis for quantitative biology. Anal Chem 78(23):7918–7925
145. Quinn DJ et al (2011) Combined simulation and experimental study of large deformation of red blood cells in microfluidic systems. Ann Biomed Eng 39(3):1041–1050

146. Diez-Silva M et al (2012) Pf155/RESA protein influences the dynamic microcirculatory behavior of ring-stage Plasmodium falciparum infected red blood cells. Sci Rep 2:614
147. Zheng Y et al (2012) High-throughput biophysical measurement of human red blood cells. Lab Chip 12(14):2560–2567
148. Huang S et al (2013) Dynamic deformability of Plasmodium falciparum-infected erythrocytes exposed to artesunate in vitro. Integr Biol 5(2):414–422
149. Wu T, Feng JJ (2013) Simulation of malaria-infected red blood cells in microfluidic channels: passage and blockage. Biomicrofluidics 7(4):44115
150. Zheng Y et al (2013) Electrical measurement of red blood cell deformability on a microfluidic device. Lab Chip 13(16):3275–3283
151. Zheng Y et al (2014) Characterization of red blood cell deformability change during blood storage. Lab Chip 14(3):577–583
152. Myrand-Lapierre M-E et al (2015) Multiplexed fluidic plunger mechanism for the measurement of red blood cell deformability. Lab Chip 15(1):159–167
153. Rosenbluth MJ, Lam WA, Fletcher DA (2008) Analyzing cell mechanics in hematologic diseases with microfluidic biophysical flow cytometry. Lab Chip 8(7):1062–1070
154. Chen J et al (2011) Classification of cell types using a microfluidic device for mechanical and electrical measurement on single cells. Lab Chip 11(18):3174–3181
155. Lee LM, Liu AP (2015) A microfluidic pipette array for mechanophenotyping of cancer cells and mechanical gating of mechanosensitive channels. Lab Chip 15(1):264–273
156. Tsai CH et al (2014) A new dimensionless index for evaluating cell stiffness-based deformability in microchannel. IEEE Trans Bio-Med Eng 61(4):1187–1195
157. Luo YN et al (2014) A constriction channel based microfluidic system enabling continuous characterization of cellular instantaneous Young's modulus. Sens Actuators B: Chem 202:1183–1189
158. Guo Q, Park S, Ma H (2012) Microfluidic micropipette aspiration for measuring the deformability of single cells. Lab Chip 12(15):2687–2695
159. Leong FY et al (2011) Modeling cell entry into a micro-channel. Biomech Model Mechanobiol 10(5):755–766
160. Guo Q et al (2012) Microfluidic biomechanical assay for red blood cells parasitized by Plasmodium falciparum. Lab Chip 12(6):1143–1150
161. Beattie W et al (2014) Clog-free cell filtration using resettable cell traps. Lab Chip 14 (15):2657–2665
162. Huang SB et al (2014) A clogging-free microfluidic platform with an incorporated pneumatically-driven membrane-based active valve enabling specific membrane capacitance and cytoplasm conductivity characterization of single cells. Sens Actuators B: Chem 190:928–936
163. Lautenschlager F et al (2009) The regulatory role of cell mechanics for migration of differentiating myeloid cells. Proc Natl Acad Sci USA 106(37):15696–15701
164. Remmerbach TW et al (2009) Oral cancer diagnosis by mechanical phenotyping. Cancer Res 69(5):1728–1732
165. Chen B, Guo F, Xiang H (2011) Visualization study of motion and deformation of red blood cells in a microchannel with straight, divergent and convergent sections. J Biol Phys 37 (4):429–440
166. Forsyth AM et al (2010) The dynamic behavior of chemically "stiffened" red blood cells in microchannel flows. Microvasc Res 80(1):37–43
167. Lee SS et al (2009) Extensional flow-based assessment of red blood cell deformability using hyperbolic converging microchannel. Biomed Microdevices 11(5):1021–1027